Development of 50-kW-Class High-Temperature Superconducting Induction/Synchronous Motor With Continuous Drive Characteristics from Room Temperature

AUTHOR(S):

Nakamura, Taketsune; Yoshikawa, Masaaki; Terazawa, Toshihisa; Matsuki, Kenjiro; Gao, Yunfei; Kiss, Takanobu

CITATION:

Nakamura, Taketsune ...[et al]. Development of 50-kW-Class High-Temperature Superconducting Induction/Synchronous Motor With Continuous Drive Characteristics from Room Temperature. IEEE Transactions on Applied Superconductivity 2023, 33(5): 5200205.

ISSUE DATE:

2023-08

URL:

http://hdl.handle.net/2433/282120

Development of 50-kW-Class High-Temperature Superconducting Induction/Synchronous Motor with Continuous Drive Characteristics from Room Temperature

Taketsune Nakamura, *Member, IEEE*, Masaaki Yoshikawa, Toshihisa Terazawa, Kenjiro Matsuki, Yunfei Gao, and Takanobu Kiss, *Member, IEEE*

***Abstract*—We investigate the rotational characteristics of a 50-kW-class high-temperature superconducting induction/synchronous motor in superconducting and non-superconducting states. The prototype motor was first placed in liquid nitrogen, and the efficiency contour was obtained. The liquid nitrogen was then gradually removed from the motor under the partial load (10 kW) condition. This showed that continuous operation is possible even at temperatures exceeding 130 K. Furthermore, we succeeded in driving at 11% of the rated output, even at room temperature. As a result, a practical high-temperature superconducting motor that can continue to operate with reduced output even when the cooling system fails could be realized.**

***Index Terms*—High-temperature superconductor, induction /synchronous motor, room-temperature operation, superconductor/normal conductor hybrid squirrel-cage winding.**

I. Introduction

THE ELECTRIC drive of transportation equipment, such as automobiles, ships, and aircraft, is considered to be an essential technology for a low-carbon society in the future [1]. In such transportation equipment, the drive motor is installed in a limited space within the moving body; thus, it is necessary to increase the mechanical output (and/or torque) per unit volume (and/or weight) as much as possible. As a candidate that satisfies these conditions, a motor using a high-temperature superconducting (HTS) conductor capable of transporting a large current with low loss has attracted considerable attention. Therefore, vigorous research and development has been carried out in ships [2]–[6], land transportation equipment [7]–[9], and aircraft [10]–[15]. Ship propulsion motors have been successfully prototyped as full-scale motors from several hundred kilowatt to megawatt classes, and rotation tests have also been conducted.

In contrast, an HTS motor must be cooled to a cryogenic temperature; however, because of its high energy density, if the critical temperature of the HTS material is exceeded owing to the failure of the cooling system, then the operation of the motor can no longer be maintained. This raises a concern with the practical use of HTS rotating machines. For example, if the electric vehicle drive motor succumbs to the above state, the vehicle must be able to reach the nearest repair shop. However, it is impractical to mount a normal-conducting motor with a superconducting motor for emergencies, mainly because the system becomes expensive, complicated, and heavy.

To overcome this limitation, Masson *et al.* have proposed safety torque generation for aircraft [11]. They designed an auxiliary torque generation at 30% of the rated torque either from the electromagnetic shield or permanent magnets located in the inductor. As an alternative solution, our group has proposed the HTS/normal conductor hybrid squirrel-cage winding for the HTS induction/synchronous motor (HTS-ISM) to realize continuous operation with reduced mechanical output in the normal conducting state [16], [17]. However, we have not succeeded in continuously driving the HTS motor with practical mechanical output from the superconducting state to the normal conducting state. This development is important in enhancing the feasibility of HTS motors for transportation equipment.

In this study, the prototype 50-kW-class HTS-ISM is first operated in liquid nitrogen (77 K), and its high efficiency rotational characteristics are demonstrated. The motor is then continuously driven at temperatures of 77 K to over 130 K under a mechanical output of 10 kW. We further explore room-temperature effects with an output of 5.5 kW.

II. Structure and Rotating Principle

A. Structure

The structure and fundamental characteristics of the 50-kW-class HTS-ISM have been reported in [9]. Fig. 1 and Table I,

Manuscript received November 13, 2022. This work was supported by JSPS KAKENHI under Grants 22H01471 and 19H05617. The fabrication of the motor was supported by JST-ALCA.
(Corresponding author: Taketsune Nakamura)
T. Nakamura, K. Matsuki, and Y. Gao are with the Department of Electrical Engineering, Graduate School of Engineering, Kyoto University, Kyoto-daigaku-katsura, Nishikyo-ku, Kyoto 6158510, Japan (e-mail: nakamura.taketsune.2a@kyoto-u.ac.jp).
M. Yoshikawa and T. Terazawa are with IMRA JAPAN Co., Ltd., 2-36, Hachiken-cho, Kariya, Aichi, 448-8650, Japan
T. Kiss is with the Department of Electrical Engineering, Graduate School of Information Science and Electrical Engineering, Kyushu University, Nishi-ku 819-0395, Japan (e-mail: kiss.takanobu.371@m.kyushu-u.ac.jp).
Color versions of one or more of the figures in this paper are available online at http://ieeexplore.ieee.org.
Digital Object Identifier will be inserted here upon acceptance.

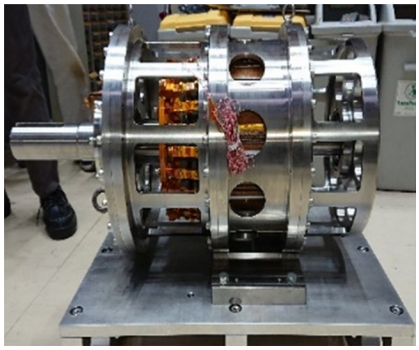

Fig. 1. Photograph of 50-kW-class HTS-ISM [9].

TABLE I
BASIC GEOMETRIC CONFIGURATIONS AND MATERIAL INFORMATION OF 50-KW-CLASS HTS-ISM

Phase number	3
Number of Poles	4
Coils per phase	12
Winding Type	Distributed winding
Slot number / conductor type of stator	60 / Copper
Conductor type of rotor	26 / BSCCO tape & No-oxygen copper
Outer diameter of stator (mm)	302.0
Inner diameter of stator (mm)	161.0
Outer diameter of rotor (mm)	160.0
Inner diameter of rotor (mm)	50.0
Length (mm)	100.0

respectively, show a photograph and basic geometric configurations as well as material information of the motor. The stator comprises a three-phase, four-pole copper winding, and the rated line voltage is 400 V. The rotor consists of squirrel-cage windings composed of bismuth-strontium-calcium-copper-oxide (BSCCO) superconductors and oxygen-free copper.

B. Rotating Principle at Superconducting and Non-superconducting States

Figs. 2(a) and (b) show a schematic diagram of a rotor bar and a squirrel-cage winding, respectively. The rotor bar consists of an HTS superconductor and normal conductor in a parallel circuit with solder connections. The primary function of the normal conductor is to mechanically reinforce the HTS conductor and secure a cooling path during heat generation. The squirrel-cage winding made of the above hybrid rotor bar is driven by a rotating magnetic field induced by a three-phase stator, i.e., the velocity electromotive force (E) is firstly generated by the rotating magnetic field as follows:

$$E = \Phi \times (2\pi r s N_s)/60, \tag{1}$$

where Φ and N_s, respectively, denote the effective value and rotating speed (synchronous speed) of the air-gap magnetic flux, and r is the radius of the rotor; s is the slip which is defined as follows:

$$s = (N_s - N) / N_s , \tag{2}$$

where N denotes the rotating speed of the rotor. The steady-

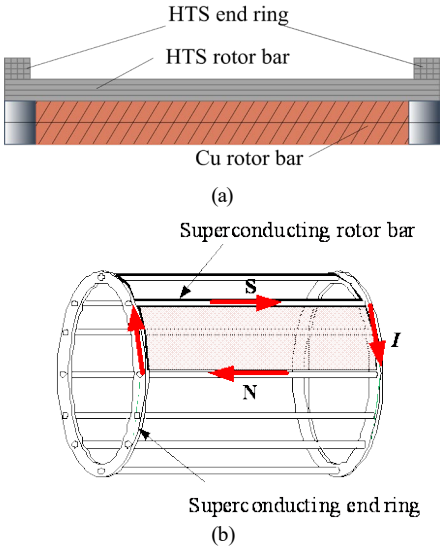

Fig. 2. Schematic diagram of rotor winding in HTS-ISM. (a) HTS conductor and oxygen-free copper hybrid rotor bar. (b) HTS squirrel-cage winding.

state rotor current (I_r) is induced by the interlinkage flux (ψ; $\psi = \Phi \times$ (turn number of rotor winding)) and the resistance of the HTS squirrel-cage winding ($R(I_r)$) as follows:

$$j\omega_{sl}\Psi + R(I_r)I_r = 0, \tag{3}$$

where ω_{sl} ($= s2\pi N_s/60$) denotes a slip angular frequency of the rotor, and j an imaginary unit. If $R = 0\ \Omega$ (superconducting state), then solving (3) yields

$$\Psi = A \text{ (const.)}, \tag{4}$$

that is, ψ is trapped in the winding and the rotor is operated at the efficient synchronous rotational mode ($s = 0$) [18]. On the other hand, ψ can also be expressed as follows:

$$\Psi = MI_s + LI_r, \tag{5}$$

where I_s, L, and M denote a stator current, self-inductance of the rotor winding, and a mutual inductance between the stator and rotor windings. When the HTS squirrel-cage winding is in flux-flow state or normal conducting state, the following equation is obtained by substituting (5) into (3):

$$I_r = -j\omega_{sl}MI_s / [R(I_r) + j\omega_{sl}L] . \tag{6}$$

If the temperature of the HTS winding rises above the critical temperature (strictly irreversible temperature), a finite resistance develops and the magnetic flux is untrapped. In this state, the rotor will rotate with the conventional slip rotation mode ($0 < s \leq 1$). Furthermore, as seen from (6), if the HTS squirrel-cage winding resistance increases as the temperature rises, the induced current decreases and the corresponding Joule type loss decreases. Essentially, we expect that a degree of negative feedback is functioned to the energy loss against temperature rise. By properly designing the normal conducting resistance, the motor can continue to operate as a normal conducting motor while maintaining a certain level of output and avoiding burnout. According to this principle, it is possible to operate even at room temperature by reducing the output.

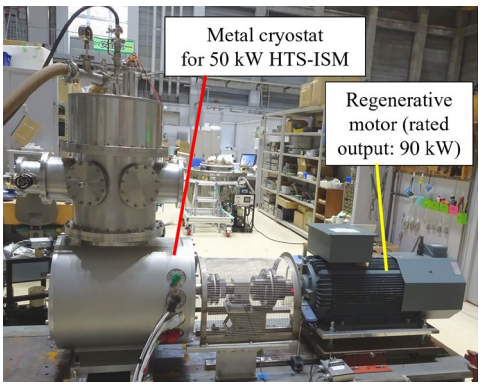

Fig. 3. Photograph of test bench.

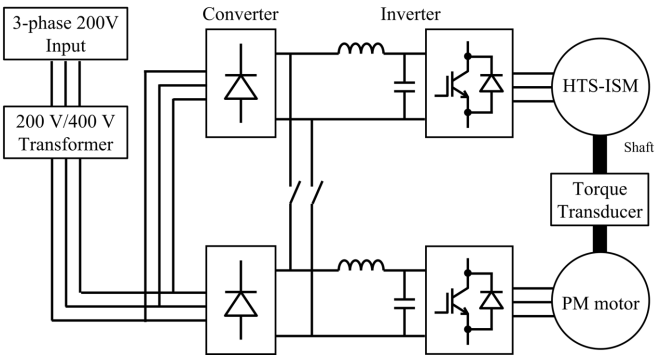

Fig. 4. Wiring diagram.

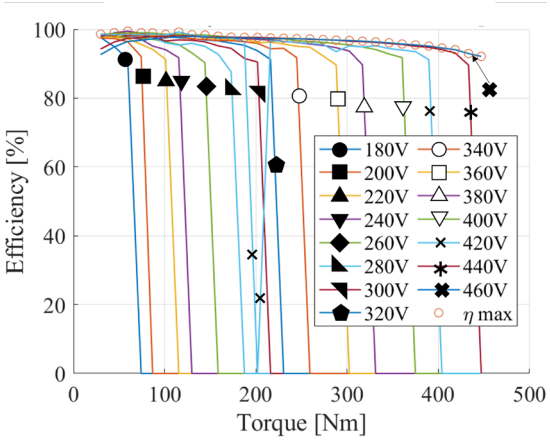

Fig. 5. Input voltage dependence of loaded curves at 40 Hz (N_s= 1200 rpm) and 77 K.

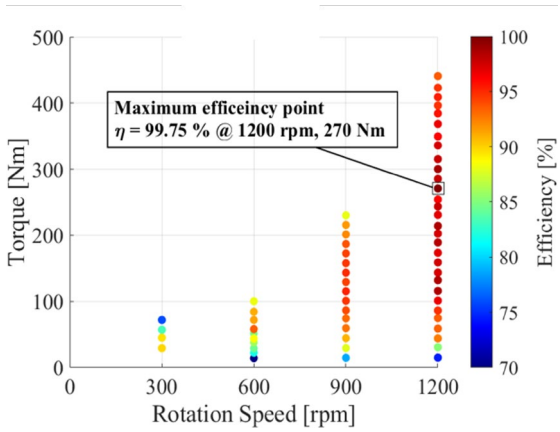

Fig. 6. Maximum efficiency contour in torque vs. rotation speed plane (77 K).

III. Rotating Test Method

A. Cryostat

The fabricated 50-kW-class motor is installed in the specially designed metal cryostat as shown in the left-hand side of Fig. 3. The motor is installed in the space immersed in atmospheric liquid nitrogen (77 K) and the stainless shaft of the rotor is connected to the room-temperature shaft. It is noted that the vacuum space is situated in between the room temperature and liquid nitrogen spaces. The upper structure of the cryostat is for maintaining liquid nitrogen in an experiment. Finally, a thermocouple is installed approximately 10 cm above the HTS-ISM.

B. Test Bench

The 50-kW-class HTS-ISM is fixed on a motor bench, and its shaft is connected to a permanent magnet regenerative motor (rated output: 90 kW) via a non-contact torque/rotation speed sensor (Fig. 3). Because the prototype HTS-ISM is of a low-speed, high-torque type, a high-output regenerative motor is required to generate the same torque.

C. Operation Method

Fig. 4 illustrates a wiring diagram for the rotation test. The 50-kW-class HTS-ISM and regenerative motor are driven by respective pulse width modulation inverters, and the input dc circuits of those inverters (470 V) are interconnected. With this circuit, the electric power absorbed by the regenerative motor is regenerated to the input circuit of the drive inverter for the fabricated HTS-ISM.

IV. Results and Discussion

A. Rotational Characteristics in Superconducting State (77 K)

Fig. 5 shows the input voltage dependence of the load characteristics at the input frequency of 40 Hz (N_s = 1200 rpm). The motor is firstly fed without a load and pulled in to run at synchronous speed. When the motor is in the steady-state rotation mode, a load is gradually applied. It should be noted that the results for the voltage of 420 V show a drop in efficiency at 200 V due to instrument error. As seen in the figure, the efficiency experiences a peak. The iron and Joule losses dominate at higher and lower speeds, respectively. The efficiency peak when both losses are equal.

The same test is repeated for a different frequency, input voltage, and load torque. The maximum efficiency is plotted for the fixed load torque and rotational speed, as shown in Fig. 6. Although the efficiency largely declines for the conventional (normal conducting) motor at the lower speed region, the fabricated motor shows higher efficiency (> 70%) even at light load (< 100 Nm) and low speed (300 rpm). Further, the effi-

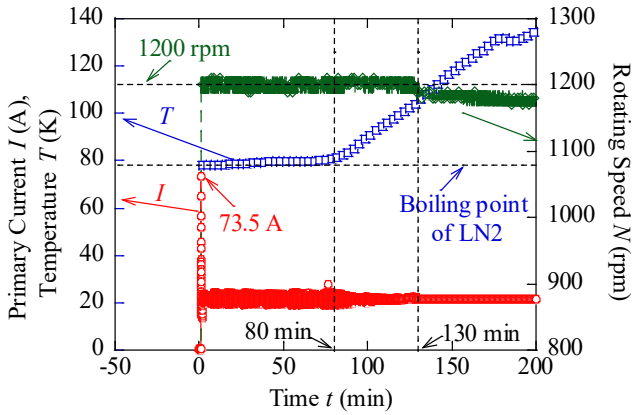

Fig. 7. Tested result of time dependence of primary current (I), rotating speed (N), and temperature (T).

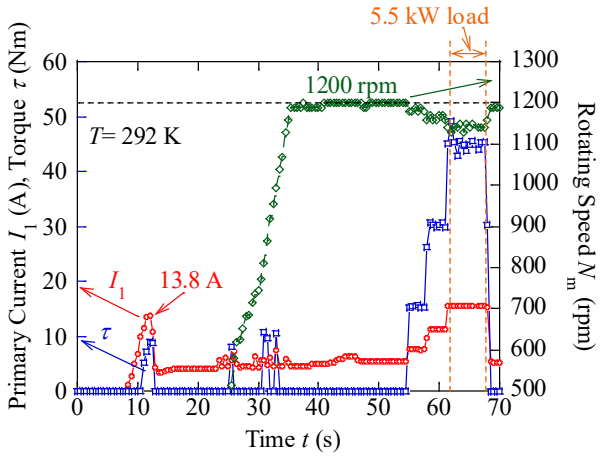

Fig. 8. Short-term room temperature load test result.

ciency reaches 99.7% at 1200 rpm and 270 Nm. However, it should be noted that the exact value of the above efficiency, including the decimal point, is not clear owing to the noise of the experimental system; this will be the subject of future research.

B. Transition Test from Superconducting State to Non-superconducting State

In this test, the motor is first excited in liquid nitrogen at a rotational speed of 1200 rpm, and a load of 10 kW (20% of the rated output) is applied. It should be noted that this test is performed in an open loop and feedback control is not conducted. After, while maintaining the operating state, the liquid nitrogen is gradually removed from the cryostat, and the rotational characteristics are continuously measured.

Fig. 7 shows the time dependence of the primary current (I), rotational speed (N), and temperature (T) with an input voltage of 400 V and input frequency of 40 Hz. The primary current increases to 73.5 A at the starting and then stabilizes at 21 A. The temperature maintains its atmospheric boiling point of liquid nitrogen for 80 min and then gradually increases at which point the liquid nitrogen is totally evaporated. On the other hand, the motor maintains its synchronous speed for 130 min and the HTS conductors maintain a superconducting state until this time. After 130 min, the rotational speed gradually slips owing to the clear normal conducting transition.

The total test time is over 3 h and there are no problems even after the normal conducting state with a 10-kW load condition. Therefore, the possibility of the continuous operation from the superconducting state to the normal conducting state is demonstrated in this test. It should also be noted that the vibration of the primary current declined after 80 min, which may be attributable to the removal of liquid nitrogen.

C. Short-Term Room-Temperature Operation

Fig. 8 shows a light load test result at room temperature (292 K). Since the room-temperature test is the first challenge, only the results for a short time (70 s) are shown in this report. First, the motor is excited with an input voltage of 300 V and input frequency of 40 Hz, and brought to a steady-state slip rotation under no-load condition. The starting current under this condition reaches 13.8 A. It is noted that the torque peaks occur four times between 10 s and 33 s at startup. This is thought to be caused by the stick-slip motion of the rotor associated with the interaction between torque generation in the shaft and friction in the bearings, but we would like to discuss the details in the future. After reaching a steady rotational speed (1198 rpm) in approximately 36 s, a load is gradually increased after 55 s. Next, a load of 5.5 kW (11% of rated output) is applied from 62 to 68 s. As shown in the figure, despite the load test at room temperature, the rotation is maintained without a temperature rise. These results demonstrate the possibility of continuous operation of HTS-ISM even at room temperature. At present, a long-term operation test is under preparation. Furthermore, based on this result, we are developing the HTS-ISM, which can generate more mechanical output at room temperature, e.g., 20% of rated power.

V. Conclusion

The rotating characteristics of the fabricated 50-kW-class HTS-ISM were tested in superconducting and normal conducting states. At 77 K, a potential maximum efficiency of over 99% was achieved. When the operating temperature was gradually increased from the boiling point of liquid nitrogen (77 K) under a partial load of 10 kW, it was confirmed that the motor could be driven continuously up to a temperature exceeding 130 K. In addition, during continuous operation for more than 3 h, no technical troubles, such as burnout of the cryostat, occurred. A short-term test with a load of 5.5 kW was successful, even at room temperature. By optimizing the design of the HTS squirrel-cage winding based on these results, an HTS motor system that can be continuously driven from room temperature will be realized and the practical technology called fail-safe function will be available.

Acknowledgment

We thank Takuro Ogasa and Jun Matsuura for their help in preparing the rotation test. We would like to thank Editage (www.editage.com) for English language editing.

REFERENCES

[1] IEA. "Transport: Improving the sustainability of passenger and freight transport" [Online]. Available: https://www.iea.org/topics/transport, Accessed on: Oct. 17, 2022.

[2] G. M. Frank, J. Frauenhofer, P. van Hasselt, W. Nick, H-W. Neumueller, and G. Nerowski, "Long-term operational experience with first Siemens 400 kW HTS machine in diverse configurations," *IEEE Trans. Appl. Supercond.*, vol. 13, no. 2, pp. 2120–2123, Jun. 2003.

[3] B. Gamble, G. Snitchler, and T. MacDonald, "Full power test of a 36.5 MW HTS propulsion motor," *IEEE Trans. Appl. Supercond.*, vol. 21, no. 3, pp. 1083–1088, Jun. 2010.

[4] A. Fukaya, T. Tsuda, and T. Oota, "Progress in motor with superconducting armature windings-axial -gap synchronous motors cooled by liquid nitrogen-," *TEION KOGAKU (J. Cryo. Super. Soc. Jpn.)*, vol. 47, no. 6, pp. 370–376, 2012 (in Japanese).

[5] H. Moon, Y-C. Kim, H-J. Park, I-K. Yu, M. Park, "An introduction to the design and fabrication progress of a megawatt class 2G HTS motor for the ship propulsion application," *Supercond. Sci. Technol.*, vol. 29, no. 3, 034009, Mar. 2016.

[6] T. Yanamoto, M. Izumi, K. Umemoto, T. Oryu, Y. Murase, and M. Kawamura, "Load test of 3-MW HTS motor for ship propulsion," *IEEE Trans. Appl. Supercond.*, vol. 27, no. 8, 5204305, Jun. 2017.

[7] H. Oyama, and T. Shinzato, "Development of high-temperature superconducting DC motor for automobiles," *Research, Fabrication and Applications of Bi-2223 HTS Wires (World Scientific)*, pp. 485–494, 2016.

[8] T. Nakamura, Y. Itoh, M. Yoshikawa, T. Nishimura, T. Ogasa, N. Amemiya, Y. Ohashi, S. Fukui, and M. Furuse, "Tremendous enhancement of torque density in HTS induction/synchronous machine for transportation equipments," *IEEE Trans. Appl. Supercond.*, vol. 25, no. 3, 5202304, Jun. 2015.

[9] A. Colle, K. Matsuki, T. Nakamura, M. Yoshikawa, Y. Ito, and T. Terazawa, "Load test and efficiency map measurement of 50 kW class induction/synchronous superconducting machine (HTS-ISM)," *IEEE Trans. Appl. Supercond.*, vol. 31, no. 4, 5202805, Jun. 2021.

[10] P. J. Masson, D. S. Soban, E. Upton, J. E. Pienkos, and C. A. Luongo, "HTS motors in aircraft propulsion: Design considerations," *IEEE Trans. Appl. Supercond.*, vol. 15, no. 2, pp. 2218–2221, Jun. 2005.

[11] P. J. Masson, P. Tixador, and C. A. Luongo, "Safety torque generation in HTS propulsion motor for general aviation aircraft," *IEEE Trans. Appl. Supercond.*, vol. 17, no. 2, pp. 1619–1622, Jun. 2007.

[12] C. A. Luongo, P. J. Masson, T. Nam, D. Mavris, H. D. Kim, G. V. Brown, M. Waters, and D. Hall, "Next generation more-electric aircraft: A potential application for HTS superconductors," *IEEE Trans. Appl. Supercond.*, vol. 19, no. 3, pp. 1055–1068, Jun. 2009.

[13] M. Boll, M. Corduan, S. Biser, M. Filipenko, Q. Huang Pham, S. Schlachter, P. Rostek, and M. Noe, "A holistic system approach for short range passenger aircraft with cryogenic propulsion system," *Supercond. Sci. Technol.*, vol. 33, 044014, 2020.

[14] Airbus. "Cryogenics and superconductivity for aircraft, explained" [Online]. Available: https://www.airbus.com/en/newsroom/stories/2021-03-cryogenics-and-superconductivity-for-aircraft-explained, Accessed on: Nov. 3, 2022.

[15] Y. Terao, A. Seta, H. Ohsaki, H. Oyori, and N. Morioka, "Lightweight design of fully superconducting motors for electrical aircraft propulsion systems," *IEEE Trans. Appl. Supercond.*, vol. 29, no. 5, 5202305, Aug. 2019.

[16] T. Nakamura, K. Nagao, T. Nishimura, and K. Matsumura, "An induction/synchronous motor with high temperature superconductor/normal conductor hybrid double-cage rotor windings," *Supercond. Sci. Technol.*, vol. 22, no. 4, 045022, Apr. 2009.

[17] H. Shimura, T. Nakamura, H. Kitano, T. Nishimura, N. Amemiya, and Y. Itoh, "Calculated characteristics of HTS induction/synchronous machine below and above its critical temperature," *IEEE Trans. Appl. Supercond.*, vol. 23, no. 3, 5201705, Jun. 2013.

[18] G. Morita, T. Nakamura, and I. Muta, "Theoretical analysis of a YBCO squirrel-cage type induction motor based on an equivalent circuit," *Supercond. Sci. Technol.*, vol. 19, no. 6, pp. 473–478, Jun. 2006.